Applied Surface Science 277 (2013) 15–24

Contents lists available at SciVerse ScienceDirect

Applied Surface Science

journal homepage: www.elsevier.com/locate/apsusc

Plasma nitriding using high H_2 content gas mixtures for a cavitation erosion resistant steel

A.N. Allenstein[a], C.M. Lepienski[b], A.J.A. Buschinelli[c], S.F. Brunatto[d,*]

[a] Programa de Pós-Graduação em Engenharia e Ciência dos Materiais (PIPE), Universidade Federal do Paraná (UFPR), 81531-990 Curitiba, PR, Brazil
[b] Departamento de Física, Universidade Federal do Paraná (UFPR), 81531-990 Curitiba , PR, Brazil
[c] Departamento de Engenharia Mecânica, Universidade Federal de Santa Catarina (UFSC), 88040-900 Florianópolis, SC, Brazil
[d] Plasma Assisted Manufacturing Technology & Powder Metallurgy Group, Departamento de Engenharia Mecânica, Universidade Federal do Paraná, 81531-990 Curitiba, PR, Brazil

ARTICLE INFO

Article history:
Received 4 December 2012
Received in revised form 11 March 2013
Accepted 11 March 2013
Available online 4 April 2013

Keywords:
Plasma nitriding
Plasma etching
High H_2 content gas mixture
CA-6NM martensitic stainless steel
Cavitation erosion

ABSTRACT

Plasma nitriding using high H_2 content gas mixtures in CA-6NM martensitic stainless steel was studied in the present work. Nitriding was performed in $H_2 + N_2$ gas mixtures for 5, 10 and 20% N_2, in volume, at 773 K (500 °C), during 2 h. Changes in the surface morphology and nitrided layer constitution were characterized by SEM, XRD, roughness analysis, and nanoindentation technique. Cavitation erosion behavior of the nitrided samples was also investigated by means of a 20 kHz ultrasonic vibrator. The study was emphasized for the three first cavitation stages (incubation, acceleration, and maximum erosion rate stage) of the cumulative erosion–time curve. Results indicate that the gas mixture nitrogen content strongly influences the phases' formation and its distribution on the nitrided layer. Better cavitation erosion resistance which was attributed to the finer and more homogeneous distribution of the nitrided layer phases was verified for samples treated at 5% N_2. Otherwise, worse cavitation erosion behavior for samples nitrided at 20% N_2 is supposed to be due to the formation of multiphase compound layer constituted by $Fe_4N + Fe_{2-3}N + CrN$, which can infer residual stress in treated surface.

1. Introduction

The soft martensitic stainless steel ASTM A743 grade CA-6NM (Fe–13%Cr–4%Ni–Mo) was developed to improve the weldability of conventional martensitic stainless steels like, for example, the ASTM CA-15 and AISI 410 steels, and to attend the needs of the market, such as superior mechanical properties and facilities to be fabricated. After tempering it presents excellent mechanical properties, as high strength, good corrosion resistance, high cavitation erosion resistance and superior ductility and toughness, even at low temperatures. Due to its high hardenability, it is utilized in diverse applications covering power generation, offshore oil and petrochemical fields, being commonly used in the manufacturing of large pieces as hydraulic turbine rotors, and pumps and compressors parts [1–4].

The microstructure of the CA-6NM steel at room temperature is usually composed of tempered-martensite with small amounts of fine carbide precipitates and a certain volume fraction of reversed or retained austenite, depending on the carbon content, austenite-stabilizing elements, and heat treatment conditions [4]. In this steel, the dominant strengthening component is the martensitic structure itself, but higher strength or better toughness is effectively related to other microstructural components such as those fine precipitates and reversed or retained austenite. In addition, when suitable tempering is applied after the steel quenching, both impact toughness and cryogenic ductility can be improved due to the formation of finely distributed reversed austenite (γ phase) along the martensite interlath boundaries [4].

In hydraulic machines parts, as turbine rotors, the cavitation phenomenon tends to be accelerated because of the long periods of time comprising continuous action of water flux and pressure variation. The region with higher water contact, as rotor blades, becomes susceptive to cavitation process. The cavitation phenomenon is characterized by vapor generation and condensation and it occurs frequently in hydraulic machines. It causes vibration, increase hydrodynamic drag, changes in the hydrodynamics flow, noise, thermal and light effects like luminescence and, the most important of all, the cavitation erosion. Rayleigh was the first to study the cavitation erosion problem on the ship propellers [5,6]. Since then many studies have been conducted in this area, comprising different materials and treatments emphasizing the surface characteristics and properties exposed to the cavitation effect.

It is to be noted that the first results covering the improvement of the surface resistance to cavitation erosion by application of the plasma nitriding technique were only recently presented [7]. Despite of this, many studies related to the plasma nitriding of 400

* Corresponding author. Tel.: +55 41 33613231; fax: +55 41 33613129.
E-mail addresses: brunatto@ufpr.br, sfbrunatto@gmail.com (S.F. Brunatto).

0169-4332/$ – see front matter © 2013 Elsevier B.V. All rights reserved.
http://dx.doi.org/10.1016/j.apsusc.2013.03.055

series (AISI) martensitic stainless steels such as the 410 and 420 alloys [8–10] have been performed emphasizing microstructure, wear and corrosion aspects of the treated materials. Compound layers presenting γ'-Fe_4N, ε-$Fe_{2-3}N$ and CrN phases and hardness up to 1500 $HV_{0.025}$ were obtained in [8], for 420 steel samples nitrided between 753 and 833 K (480 and 560 °C), during 4 h, for a gas mixture of 75% N_2 + 25% H_2, and pressure of 250 Pa (1.87 Torr). Samples of 410 steel were plasma nitrided in [9], between 623 and 773 K (350 and 500 °C), for long nitriding times up to 28 h, using a gas mixture of 25% N_2 + 75% H_2. Compound layer presenting expanded ferrite phase (α_N) and incipient precipitation of γ'-Fe_4N was observed for samples nitrided at 623 K. Electrochemical measurements indicate decrease of the corrosion resistance for samples nitrided during 20 h, at 673 and 773 K, but low corrosion current or better corrosion potential was observed for samples nitrided at 623 K. Finally, the influence of low temperature plasma nitriding on the wear and corrosion resistance of 420 steel was investigated in [10]. Experiments were performed between 623and 823 K (350 and 550 °C), for 15 h, using a gas mixture of 25% N_2 + 75% H_2. Both the corrosion and the wear resistance of the samples treated at 623 K were improved, due to the combined effect in keeping Cr solved in the steel matrix and by forming high chemical stability phases (α_N and ε-Fe_3N) at the steel surface. However, reduced corrosion resistance was verified for samples treated at 723 and 823 K due to formation of CrN in the nitrided layer.

Otherwise, little or nothing has been published up to now comprising plasma nitriding of soft martensitic stainless steels, which is the case of the CA-6NM alloy. So, this is to be extensively explored and stressed, keeping in mind that, confronting with the 400 series steels, CA-6NM additionally presents Ni and Mo in its composition, and retained-austenite fraction in its constitution.

On the other hand, it is well known that the sputtering caused by plasma species bombardment effect can lead to modifications of surface characteristics and finishing of parts processed in DC (direct current) glow discharges. In this case, the higher the use of heavier species fractions in H_2 + N_2 gas mixtures the higher is the sputtering effect on the plasma exposed surface. In addition, allied to it, gas mixture is another aspect that deserves special attention in plasma assisted treatments of stainless steels due to the presence of a stable chromium oxide layer on the steel surface. This assertion is based on the strong reductor characteristic of the hydrogen gas, as verified in [11–13]. Despite the large use of N_2 + H_2 gas mixtures in plasma nitriding studies for N_2 contents varying between 20 and 90% in volume, as evidenced in [8–10], it is to be also explored the use of high H_2 contents (>80% H_2) in the treatment of stainless steels. So, considering the above-mentioned aspects, surface change of a cavitation erosion resistant steel obtained for a short plasma nitriding time (2 h) was investigated in the present work as a function of the H_2 + N_2 gas mixture, for low nitrogen contents (5–20% N_2, in volume), aiming to determine its effect on the morphology and constitution of the nitrided layer, and the cavitation erosion behavior of the CA-6NM steel treated surface.

2. Materials and methods

Fig. 1 consists of an *in situ* internal view of the discharge chamber and the schematic representation of the cathode structure. The picture shows in detail the anode structure surrounding the cathode structure. The scheme also shows the cathode structure, which is comprised by the sample, thermocouple holder, thermocouple and insulating component.

The discharge chamber consisted of a 350 mm diameter, 380 mm high stainless steel cylinder attached to steel plates and sealed with o-rings at both ends. The system was evacuated to a residual pressure of 1.33 Pa (10^{-2} Torr) using a two stage

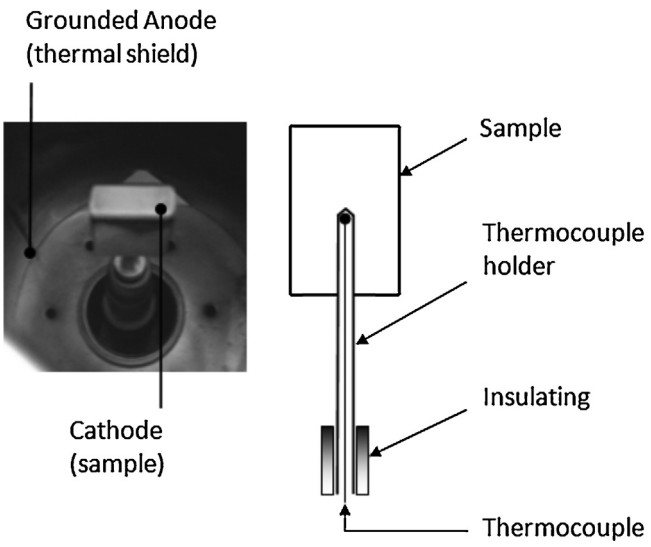

Fig. 1. *In situ* internal view of the discharge chamber and the schematic representation of the cathode structure.

mechanical pump. The gas mixture of N_2 and H_2 was adjusted by mass flow controllers of 8.33×10^{-6} m^3 s^{-1} operating at full scale, respectively. The pressure in the vacuum chamber was adjusted with a manual valve and measured with a capacitance manometer of 13.3×10^3 Pa (100 Torr) in full-scale operation.

Samples in dimensions of 30 mm × 20 mm × 10 mm were machined from a ASTM A743 grade CA-6NM martensitic stainless steel, a typical material utilized in manufacturing of Francis turbine rotors, which was received in the tempered condition for hardness of 22 HRC. Table 1 shows the expected composition for the referred steel in accordance with ASTM standard, and the average composition of the start material utilized in the present study.

The sample, presenting a blind hole (15 mm length and 5 mm diameter), was placed on an AISI 1008 carbon steel support (40 mm height and 5 mm diameter) that served as the cathode in the electrical system and the thermocouple support (see Fig. 1). Both the 30 mm × 20 mm surfaces of the sample were handy polished using 320, 400, 600 and 1200 grade sandpaper in high rotation machine, and finished by polishing using 1.0 μm Al_2O_3 + water solution.

Cathode was negatively biased at the voltage, using a square form pulsed power supply. The voltage was set to 660 ± 15 V. To ensure a stable discharge, an electrical resistance was connected in series between the power supply and the discharge chamber. The power transferred to the plasma was adjusted by varying the time that the pulse was switched on (*ton*). The pulse period used was 240 μs. The temperature of the sample was selected by adjusting the on/off time of the pulsed voltage. Temperature was measured by means of a chromel–alumel thermocouple (type K of 1.5 mm diameter), placed inside the thermocouple holder, which is inserted to a depth of 15 mm into the sample (see Fig. 1).

Nitriding was performed at 773 K (500 °C), during 2 h, at 532 Pa (4 Torr), with a gas flow of 5×10^{-6} m^3 s^{-1} (in accordance with [14]), for three different gas mixtures: (a) 5% N_2 + 95% H_2; (b) 10% N_2 + 90% H_2; and (c) 20% N_2 + 80% H_2 (in volume).

The procedure of the nitriding was divided into three steps:

(i) sample was cleaned under a H_2 electrical discharge at 623 K (350 °C) for 10 min, using 399 Pa (3 Torr) pressure and the resistance adjusted to 50 Ω;
(ii) sample was nitrided at specified temperature, using 532 Pa (4 Torr) pressure and resistance adjusted to 50 Ω;
(iii) sample was cooled under a gas mixture flow.

Table 1
Chemical composition (in wt.%) of the studied steel according to ASTM A743 CA-6NM standard and the studied samples.

Composition (wt.%)	C	Mn	Si	Cr	Ni	Mo	P	S
ASTM A743 CA-6NM	$0.060_{max.}$	$1.00_{max.}$	$1.00_{max.}$	11.5–14.0	3.5–4.5	0.4–1.0	$0.04_{max.}$	$0.03_{max.}$
Sample	0.032	0.63	0.522	12.25	4.42	0.43	0.024	0.015

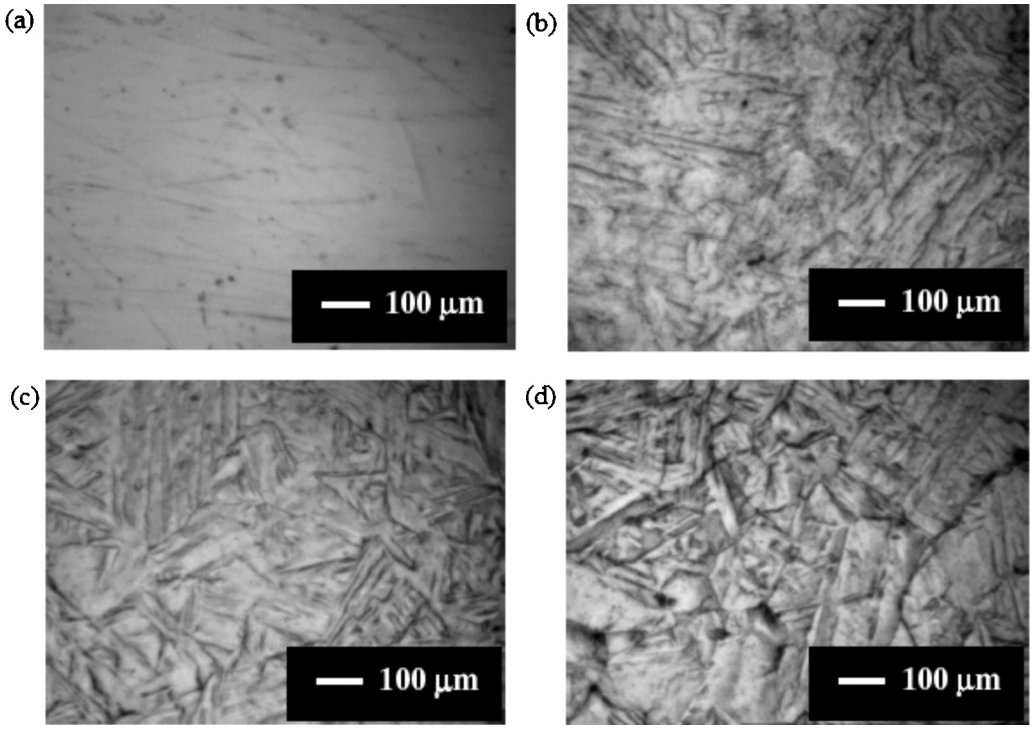

Fig. 2. Surface aspect of the substrate material in the: (a) start condition (as non-nitrided); and plasma nitrided at (b) 5; (c) 10; and (d) 20% N_2.

Characterization was carried out on the 30 mm × 20 mm sample side. The surface morphology of the samples after nitriding was characterized using the optical system present in a XP-MTS nanoindenter. The same equipment was used to determine hardness and elastic modulus of the treated surface. The nanoindentation technique was carried out using Berkovich indenter, loads up to 40 g (400 mN), for eight loadings using 10 s loading time. X-ray diffractometry (XRD) was performed on the studied surfaces to determine the phases of the nitride layer, by using a Shimadzu equipment and copper tube with wave-length of 1.54 nm, for θ–2θ (Bragg–Brentano) configuration. Scanning electron microscopy (SEM) was realized in a FEI-Quanta microscope aiming to determine the microstructure of the nitride layer and characteristics of the cavitation eroded surfaces. Chemical composition of phases present in nitride layer was obtained by means of energy dispersive X-ray microprobe analysis (EDX). As the EDX technique is not adequate to quantify light components as nitrogen, the indicated measurements are presented only for qualitative purpose. Finally, sputtering effects on treated surfaces were quantified by means of roughness determination. Measurements of roughness were conducted in accordance with ISO 4287 (1997) for *Ra* and *Rz* determination. In this case, it was utilized a Mahr-Concept equipment, with filter Gauss, 4 mm measurement length and 0.80 mm wave length (five divisions).

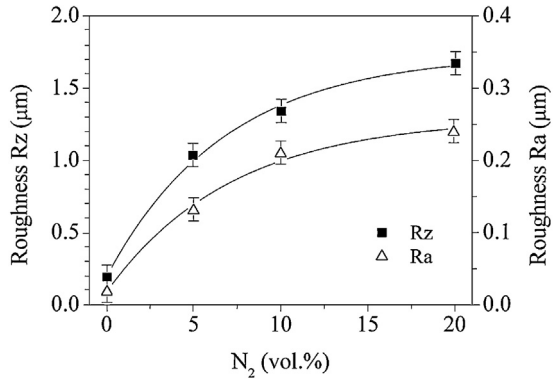

Fig. 3. Quantitative determination of the sputtering effect by *Ra* and *Rz* roughness measurement (the point related to 0% N_2 represents the surface in its start condition as non-nitrided).

The cavitation experiments were made in a standard vibratory cavitation erosion tester as a function of testing time, according to ASTM G 32-09, as described in details in [15]. Samples were cavitated in ultrasonic vibratory equipment *via* indirect method and the mass loss of the test specimens was determined by means of 0.1 mg precision balance.

3. Results and discussion

3.1. Characterization of the studied materials

Surface aspect of the substrate material in the start condition as non-nitrided, and plasma nitrided at 5, 10, and 20% N_2 are shown in Fig. 2a–d, respectively. The surface morphology was evidenced by plasma species bombardment as a consequence of the sputtering effect. Microstructure of the stainless steel comprised by tempered-martensite is better evidenced as the N_2 content in discharge was increased, resulting in the effect known as plasma etching. It is to

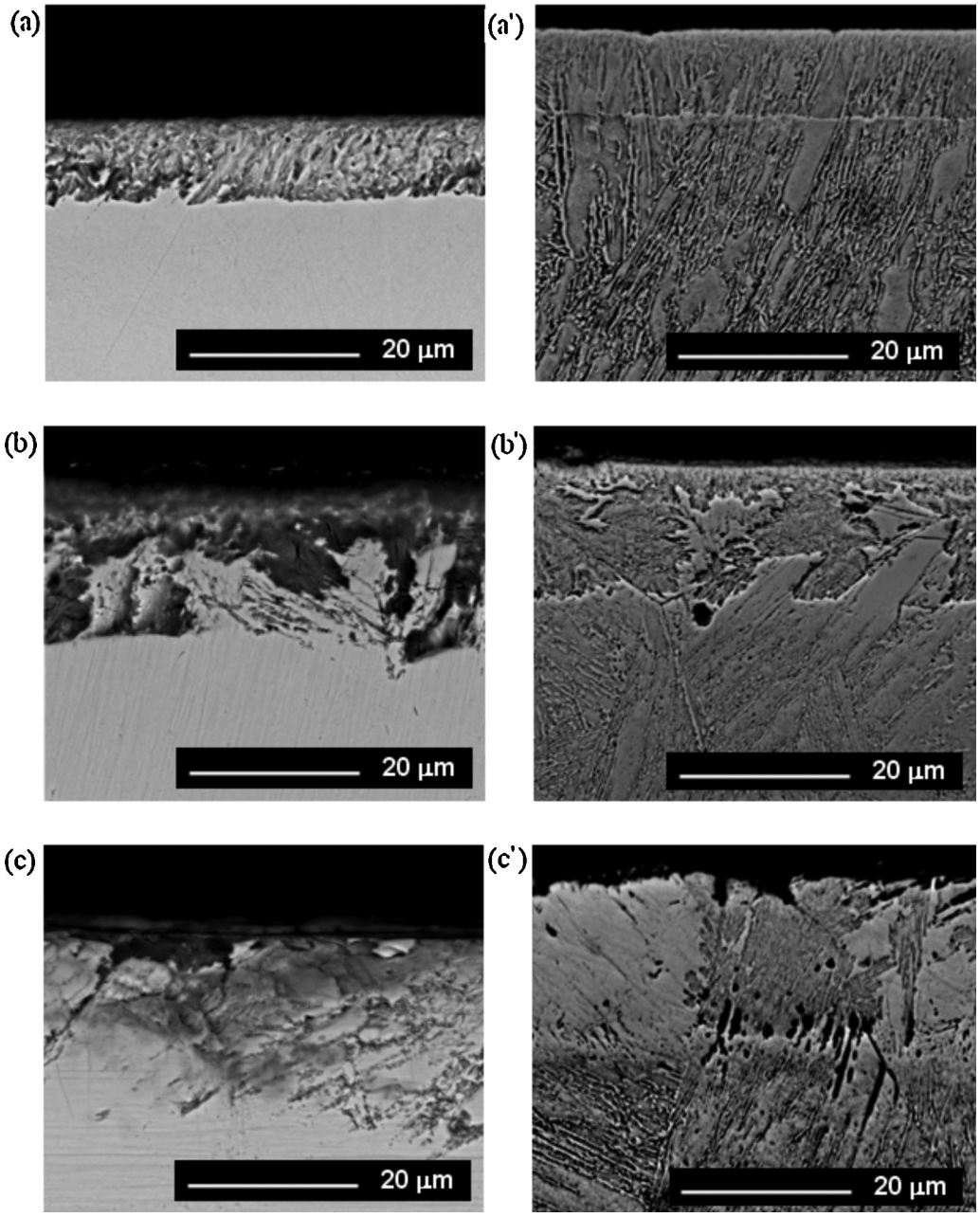

Fig. 4. SEM micrograph showing the nitrided layer etched with Nital 2% (a–c) and Marble's etchant (a′–c′) for samples treated at: (a and a′) 5; (b and b′) 10; and (c and c′) 20% N_2.

be noted that the cavitation erosion resistance is directly related to the start surface condition, and roughness measurements have been utilized to evaluate different stages of the cavitation erosion [16,17].

Quantitative determination of the sputtering effect by *Ra* and *Rz* roughness measurements are presented in Fig. 3. Results indicate the higher the N_2 content in discharge the higher is the average values for *Ra* and *Rz* roughness. The *Ra* and *Rz* average values were 0.02, 0.13, 0.21 and 0.24 μm, and 0.19, 1.03, 1.34 and 1.67 μm for surfaces in the start condition, and nitrided at 5, 10, and 20% N_2, respectively.

On the other hand, from Davis and Vanderslice (1963) study, presented in [18], the effect of the gas pressure on the ion energy distribution tends to be small if the discharge voltage is kept constant, which is the present case. So, the above mentioned results comprising the sputtering effects on treated surface could be simply explained by the higher amount of heavy species (in this case, nitrogen species when compared with hydrogen) as the N_2 content is increased in the discharge gas mixture. In this way, the average time switched-on (*ton*) utilized to keep the specified nitriding temperature at 773 K (500 °C) was decreased as the N_2 content was increased. The *ton* value of 175, 160, and 125 μs was verified for nitriding carried out at 5, 10, and 20% N_2, respectively. This result is in accordance with the higher content of heavy species in gas mixture and the effect of the plasma species bombardment on the heating of sample.

Fig. 4 shows SEM micrographs of the nitrided layer etched with Nital-2% (Fig. 4a–c), and Marble's etchant (Fig. 4a′–c′), for samples treated at 5, 10, and 20% N_2, respectively. Nital-2% was chosen to evidence changes in the original steel microstructure due to nitrogen diffusion from surface into the sample bulk, since it does not etch alloys as stainless steels in its original composition

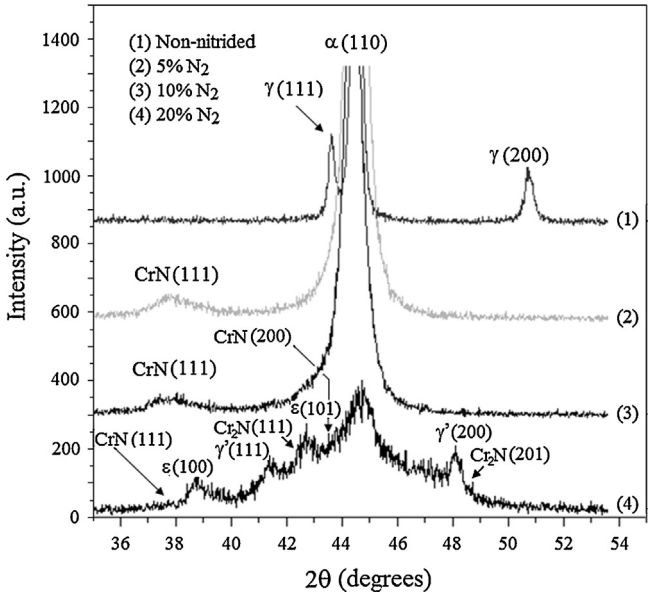

Fig. 5. XRD patterns for the studied surface: (1) as non-nitrided; and nitrided at (2) 5; (3) 10; and (4) 20% N_2.

condition, and so in the unaltered matrix of the steel, according to results of Fig. 4a–c. In this case, only the nitrided layer was revealed for all studied conditions, indicating that the steel was nitrogen-sensitized in treated layer, differently of the nitrogen-free matrix, which remains with unrevealed aspect. Layer thickness on the order of 12.5, 20 and 25 μm was verified for samples nitrided at 5, 10, and 20% N_2, respectively. On the other hand, Marble's etchant was used to reveal the whole microstructure, constituted by nitrogen-altered surface and the substrate bulk, as shown in Fig. 4a′–c′. Results indicate that the gas mixture nitrogen content can influence the phase formation and its distribution on nitrided layer. It is to be noted that the nitrided layer presents regions of distinct aspects, shadow and white, characterizing the occurrence of different phases (Fig. 4a–c).

Fig. 5 shows XRD patterns for the studied surfaces. The substrate material (as non-nitrided) presents tempered martensite (α-1 1 0) and austenite (γ-1 1 1 and γ-2 0 0) phase peaks. The patterns obtained for samples treated at 5, and 10% N_2 evidence peaks of CrN phase in addition to the nitrogen-containing tempered martensite phase (α-1 1 0). For samples treated at 20% N_2 gas mixture, the diffraction patterns suggest peaks of iron and chromium nitrides (probably γ′-Fe_4N, ε-$Fe_{2-3}N$, CrN) beyond nitrogen-containing tempered martensite or b.c.c. ferrite (α-1 1 0), a result directly related to the higher nitrogen content in the gas mixture. On the other hand, the absence of iron nitride formation for samples treated at 5, and 10% N_2 could be explained by the high chromium-to-nitrogen affinity. For these two glow discharge conditions, the smaller amount of nitrogen species in the plasma would lead to smaller amounts of atomic nitrogen diffusing into sample surface. As the chromium presents some mobility at the nitriding temperature and it is a strong nitride former, most of the diffusing nitrogen portion would combine with chromium, leading probably to the formation of CrN phase, being that the other portion would eventually remain in solid solution in the tempered martensite. In other words, the nitrogen gradient developed on sample surface would be enough to nucleate and grow stable nitride phase (CrN), keeping in mind that the iron nitrides are metastable phases. This result is strongly supported by base aspects in the prediction of the nitrided case depth of high alloy steels like stainless steels presented in [19], as follows: (a) nitrogen does not diffuse across the nitriding front until all alloy elements have been combined with nitrogen to form nitride precipitates; (b) the contribution of nitrogen dissolved in b.c.c. ferrite (or b.c.c. tempered martensite) to the total nitrogen in the nitrided case tends to be negligibly small; (c) increasing the Cr content in the steel increases the total nitrogen concentration in the nitrided case; (d) the precipitation of CrN consumes a part of the diffusing nitrogen, and thus affects the nitrogen gradient in ferrite at the nitriding front, thus slowing down nitrogen diffusion in ferrite and development of the nitrided case; (e) by reducing the nitrogen gas content in the gas mixture and thus reducing the nitrogen activity in the plasma, precipitation of different nitride phases in the nitrided case can be controlled, being that only the most stable nitride phase in a complex alloy system could be expected to occur (an result evidenced here in the XRD results for samples nitrided at 5% and 10% N_2 gas mixtures, showing the presence of CrN as a second phase); (f) as the nitrogen activity in the plasma is reduced, the equilibrium surface nitrogen concentration is built up more slowly, so much so that for a nitriding atmosphere containing too small N_2 gas content, the equilibrium surface nitrogen concentration cannot be reached even after long nitriding times [19], thus achieving bright nitriding [19–21]; and (g) during the course of nitrogen diffusion, the alloying elements in the steel such Cr combine with the diffusing nitrogen to precipitate fine scale alloy nitrides in the diffusion zone, inducing precipitation hardening [19].

On the other hand, the nitrided layer obtained at 5% N_2 presents finer distribution of phases than the other studied conditions, as evidenced in Fig. 4a by using Nital-2% as etchant, and a well defined line separating the nitrided layer and the substrate bulk, in accordance with Fig. 4a′ by using Marble's etchant. The constituent of shadow aspect distributed all over the nitrided layer is supposedly associated with CrN precipitation (Fig. 4a), being that the surrounding phase of white aspect is probably nitrogen-containing tempered martensite (or b.c.c. ferrite). It is to be observed that for the characterization conditions utilized in Fig. 4a′ the CrN precipitation is not evident. In addition, confronting both Fig. 4a and a′ results, it is evidenced that the original acicular structure of the tempered martensite is maintained practically unaltered (Fig. 4a′), differently from the observed for the other studied conditions (Fig. 4b, b′, c, and c′). So, the constituent of shadow aspect shown in Fig. 4a should not correspond to the CrN phase only. In this case, a two-phase constituent supposedly comprising high density of CrN phase strongly dispersed in nitrogen-containing tempered martensite, probably in nanometer-scale size, could be considered in the nitrided case. This assumption is supported by results presented in [22], for a gas nitriding study of a ferritic commercial steel, reporting the existence of new nitrogen-alloying-elements-containing phases of nanometer-scale size, in the treated surface.

To finish, as shown in Fig. 5, the austenite peaks present in the start material disappear for all nitriding conditions. It is assumed that the austenite transforms to martensite, since it becomes unstable at the nitriding temperature, considering further that the nitrogen-expanded austenite is known to revert to CrN + ferrite beyond 450 °C.

Figs. 6 and 7 show curves of hardness and elastic modulus as a function of the indentation depth obtained by means of nanoindentation technique, respectively. The large dispersion of measurements could be explained by surface roughness, which is a consequence of the sputtering effect, as previously discussed. The hardness results ranging between 10 and 16 GPa, presented in Fig. 6, confirm the strengthening effect of the nitrogen in high chromium steels, which is the case of the martensitic stainless steel studied here. In general, the hardening effect as a function of the gas mixture seems to be identical with only the layer thickness itself depending on the nitrogen supply, thus pointing indirectly to similar nitrogen contents in the obtained layers. But it is worth to observe that the indicated hardness measurements correspond to indentation

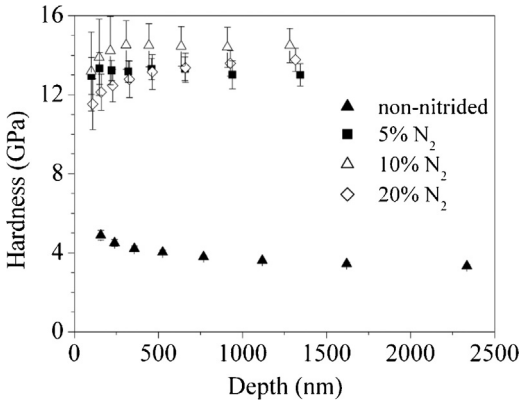

Fig. 6. Hardness × depth (of indentation) curve obtained by nanoindentation technique at surface as non-nitrided and nitrided at 5, 10 and 20% N_2.

depths on the order of 1250 nm (or 1.25 μm) only, which is about 10–20 times smaller than the thickness of the obtained nitrided layers. So, for comparison purpose, Vickers microhardness measurement using a load of 500 g was performed on treated surfaces, and hardness of 950, 1170 and 1240 $HV_{0.5}$ was verified for samples nitrided at 5, 10 and 20% N_2, respectively (results not shown). Differently, this result would indicate surface hardness differences, even slight, as a function of the nitrogen content in plasma, thus pointing indirectly to different nitrogen contents in the treated surfaces, as could be expected for different nitrogen activities in the glow discharge. Considering that the higher the nitrogen gas content in the gas mixture the higher is the nitrogen activity in the plasma, deeper and harder nitrided layers could be expected, in accordance with the tendency evidenced in the present case.

Finally, slight differences for the elastic modulus measurements can be noted in Fig. 7. For all the studied conditions, including the start material as non-nitrided, elastic modulus on the order of 250 GPa, on average was determined. The results for elastic modulus of the nitrided cases (Fig. 7) agree roughly with that obtained for hardness in Fig. 6, by nanoindentation technique. It should be noted that harder surfaces tend to be brittle, and, differently, tougher surfaces usually present better cavitation erosion resistance, as it will be considered in the sequence of the work.

3.2. Cavitation erosion behavior of plasma nitrided samples

Fig. 8 presents the cumulative mass loss (CML) as a function of the cavitation erosion time for the studied samples. It was evidenced that the cavitation erosion behavior of the CA-6NM steel

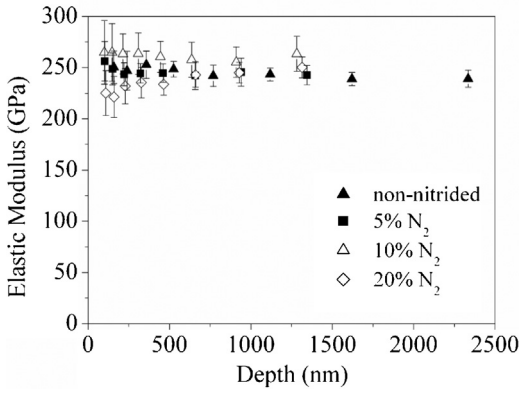

Fig. 7. Elastic modulus × depth (of indentation) curve obtained by nanoindentation technique at surface as non-nitrided and nitrided at 5, 10 and 20% N_2.

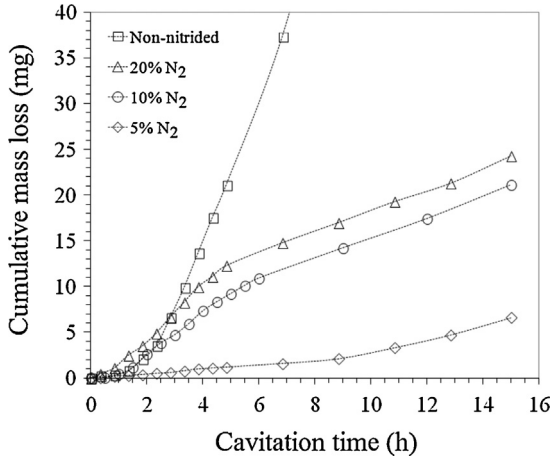

Fig. 8. Cumulative mass loss (CML) as a function of the cavitation time for the studied samples, at surface as non-nitrided and nitrided at 5, 10 and 20% N_2.

plasma nitrided samples tends to be related to the nitrogen content in $N_2 + H_2$ gas mixtures and, so, to the characteristics of the nitrided layer. This assumption is based on the fact that for the first testing times including the incubation and the acceleration stages of the CA-6NM [15], the CML up to 2.8 h testing time for the sample nitrided at 20% N_2 was higher than that verified for material in its start condition as non-nitrided, differently from the observed for samples nitrided at 5, and 10% N_2. A similar CML up to 2.4 h testing time was observed for sample nitrided at 10% N_2 and the CA-6NM steel in the start condition, as non-nitrided. Finally, very small CML up to 3.0 h testing time was observed for sample nitrided at 5% N_2. On the other hand, after the acceleration stage, in the maximum erosion rate stage of the studied samples, for testing time higher than 2.8 h, all nitriding conditions lead to smaller CML than the CA-6NM steel in its start condition as non-nitrided. In brief, at least to the studied conditions in this work, the lower the nitrogen content in $N_2 + H_2$ gas mixture the lower is the CML of the nitrided sample. It is to be noted that the worse cavitation erosion behavior in incubation and acceleration stages of the nitrided layer obtained at 20% N_2 is probably due to the constitution of the compound layer and its higher hardness, as previously discussed, exhibiting lower toughness and thus poor cavitation resistance. In addition, a multiphase compound layer tends to present residual stress in nitrided case [21,23]. The occurrence of residual stress in a multiphase structure would be probably due to the fact that the obtained phases γ′-Fe_4N, ε-$Fe_{2-3}N$, and CrN present different thermal expansion coefficients, thus they shrink differently as the sample is cooled from the nitriding to the room temperature under the gas mixture flow. Otherwise, the good behavior of the nitrided layer obtained at 5% N_2 would be related to the finer and more homogeneous distribution of the CrN dispersed in the nitrogen-containing tempered martensite matrix, according to Fig. 4a and a′ results, allied to the absence of iron nitrides, and its smaller hardness, remembering that α-Fe (or b.c.c. tempered martensite) saturated in nitrogen is tougher than γ-Fe_4N, and ε-$Fe_{2-3}N$, which could explain its higher toughness and cavitation resistance than that obtained to the other studied conditions.

3.3. Characteristics of the eroded nitrided surfaces

Surface aspect of CA-6NM steel in the start condition, as non-nitrided, for cavitation testing time of 1, 3, 7 and 15 h is shown in Fig. 9a–d, respectively. Changes in the surface morphology when compared with the start aspect of the sample, as shown in Fig. 2a, can be observed even at 1 h, since pits and undulations become

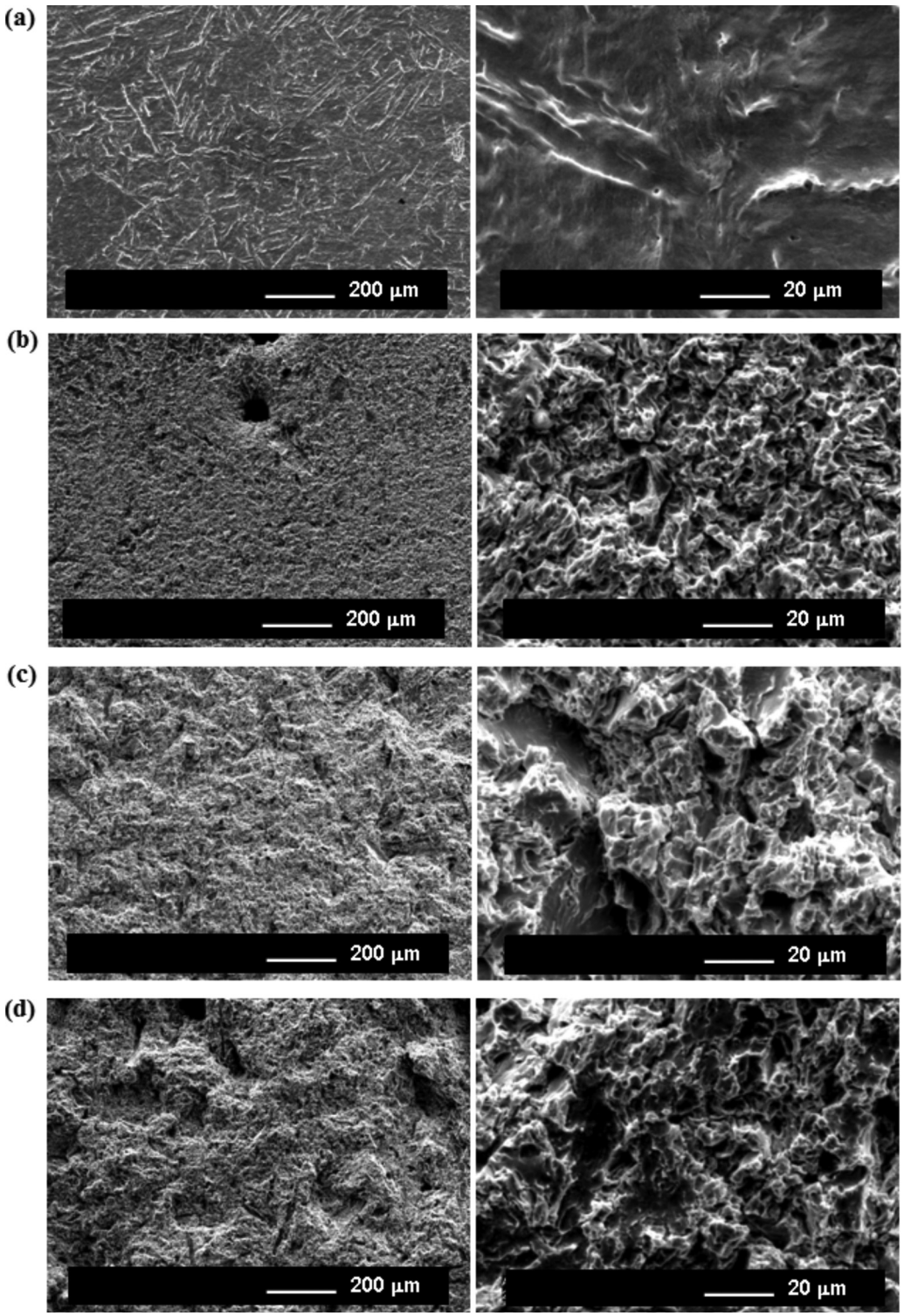

Fig. 9. Surface aspect of the substrate sample in the start condition as non-nitrided, for cavitation testing time of: (a) 1; (b) 3; (c) 7; and (d) 15 h, for two different magnifications.

apparent (Fig. 9a). The transition between incubation and acceleration stage was verified after testing time of 1 h, resulting in increase of pits and undulations. From observation of Fig. 9b–d, it was evidenced that the longer the testing time the higher is the cavitation damage of the surface. At 3 h, a surface of rougher aspect due to formation of very small craters in profusion indicates that the maximum erosion rate stage was reached (Fig. 9b). At 7 h (Fig. 9c) and 15 h (Fig. 9d), craters increase in width as well as in height, resulting in a strongly eroded surface.

Fig. 10a–d shows the surface aspect of the sample nitrided at 5% N_2, for cavitation testing time of 1, 3, 7 and 15 h, respectively. At 1 h (Fig. 10a), surface morphology of the nitrided sample remains practically unaltered, considering its start aspect obtained after nitriding (Fig. 2b). In this case, fracture of very small debris (of white aspect) can be observed at surface, too small pits in few amounts were formed, and no undulations were evidenced. As the testing time was increased for 3 h (Fig. 10b), the surface aspect was maintained similar to that observed at 1 h, *id est*,

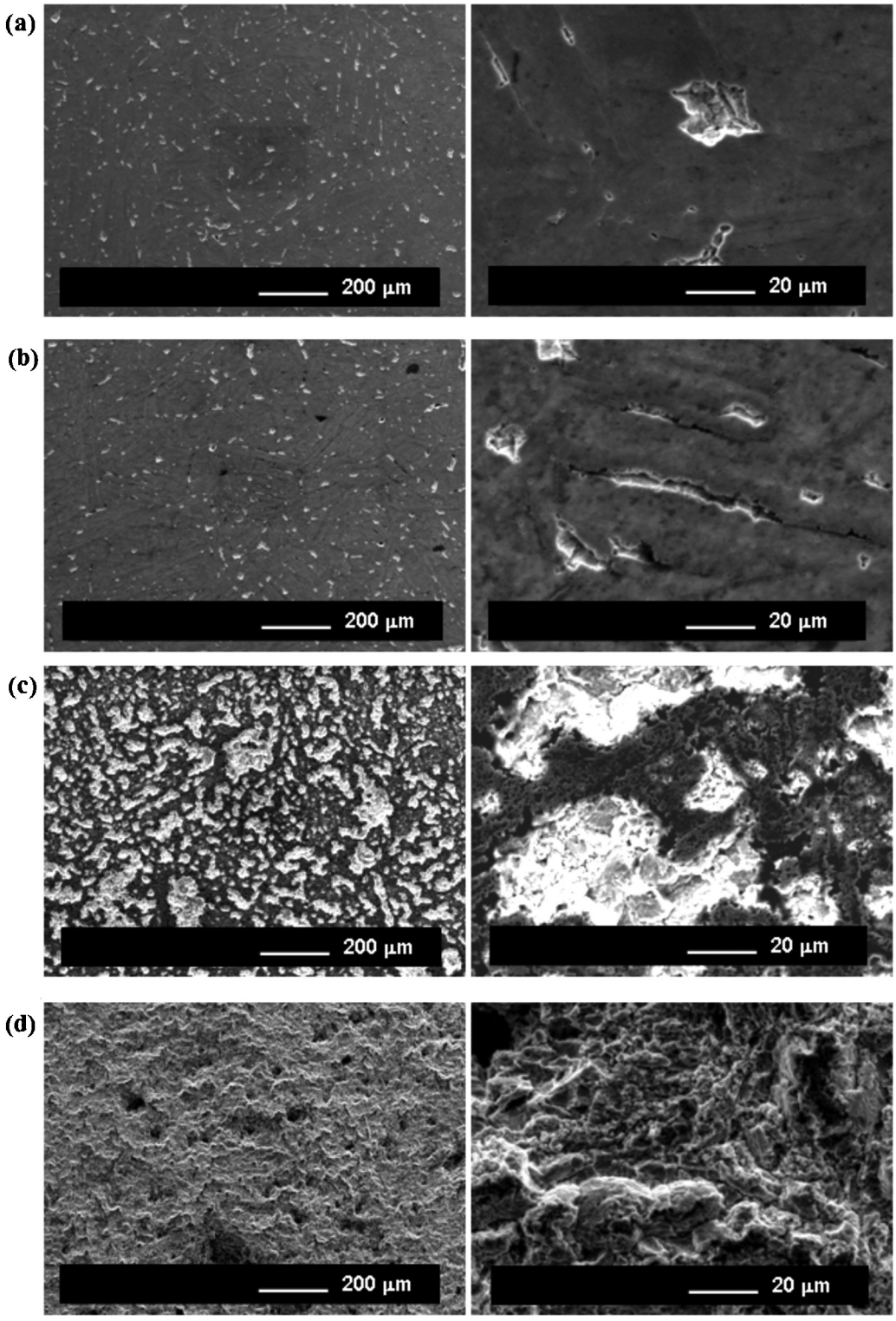

Fig. 10. Surface aspect of sample nitrided at 5% N_2, for cavitation testing time of: (a) 1; (b) 3; (c) 7; and (d) 15 h, for two different magnifications.

no undulations were noted, the formation of pits was slightly increased, and the beginning of microcracks nucleation becomes apparent. In addition, it can be observed that microcracks tend to be nucleated at the interface of the original martensite needles, in accordance with the higher magnification micrograph. The transition between incubation and acceleration stage was verified after testing time of 3 h. It is to be noted that the occurrence of no undulations is an indicative that the surface was strongly strengthened by nitrogen alloying, which is confirmed by results previously discussed in Figs. 6 and 7.

On the other hand, an interesting result was obtained at 7 h, as shown in Fig. 10c. It clearly indicates the increment of the crater formation effect (presenting white aspect), which is due to microcracks formation and fracture of debris at the surface. In addition, a high density of pits all over the tested surface, of shadow aspect, confirms that the maximum erosion rate stage has been

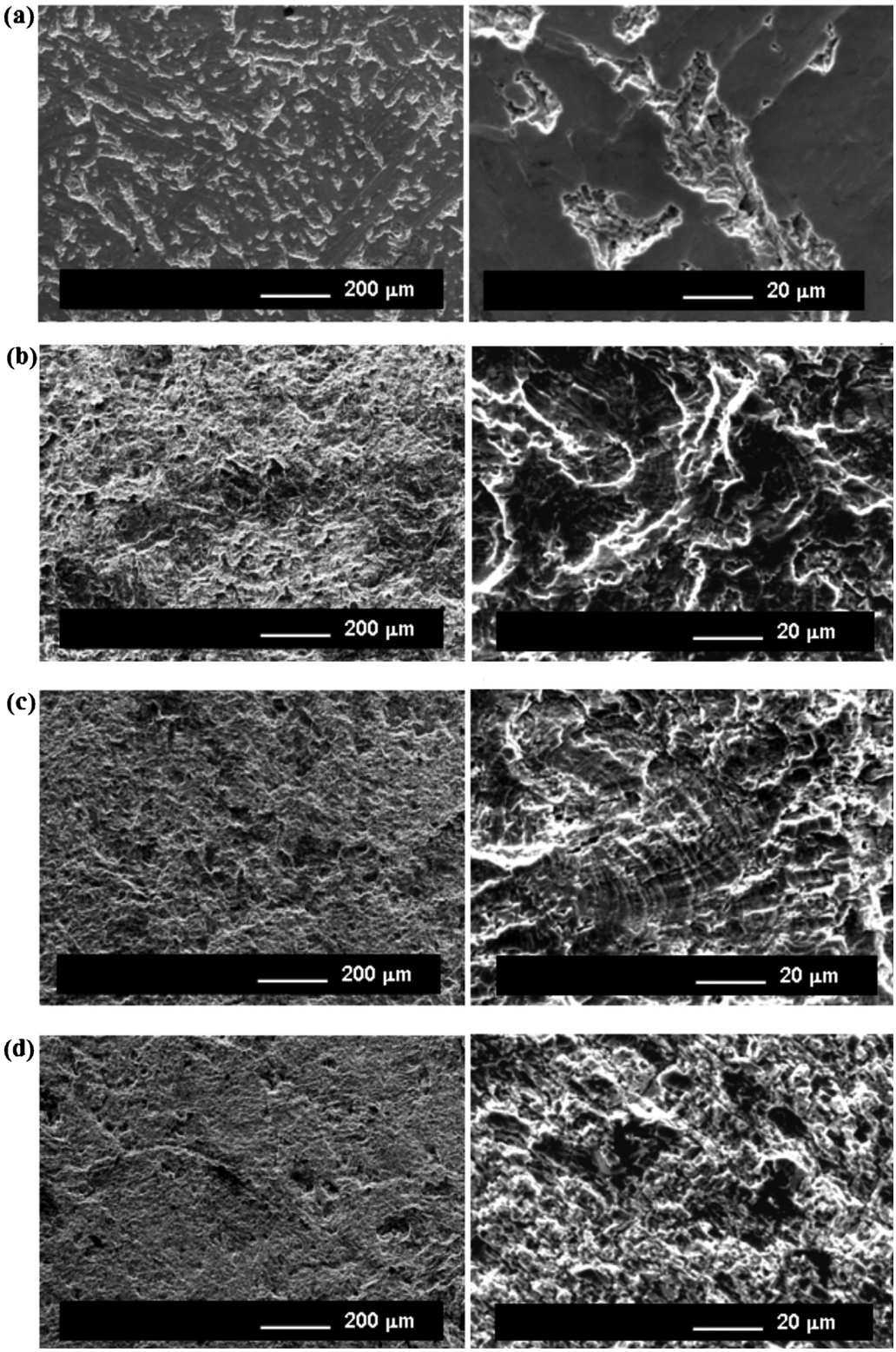

Fig. 11. Surface aspects of sample nitrided at 20% N_2, for cavitation testing time of: (a) 1; (b) 3; (c) 7; and (d) 15 h, for two different magnifications.

just reached in nitrided layer. Finally, at 15 h (Fig. 10d), strongly eroded surface was evidenced.

Surface aspect of the sample nitrided at 20% N_2, for cavitation testing time of 1, 3, 7 and 15 h is shown in Fig. 11a–d, respectively. At 1 h (Fig. 11a), strong alteration of the start surface morphology obtained after nitriding (Fig. 2d) can be evidenced, due to the intense effect of fracture of debris (of white aspect). In addition, some pits in few amounts are present. As expected, the high hardness of the nitrided surface (Fig. 6) and the occurrence of multiphase compound layer (Fig. 5) probably presenting high residual stress imply in very low toughness, which explain the occurrence of no undulations, the brittle behavior, and the worse cavitation erosion behavior of the treated surface, as discussed in Fig. 8. At 3 h (Fig. 11b), craters are present all over the tested surface,

confirming that the maximum erosion rate stage was reached in nitrided layer, being that he same was verified at 7 (Fig. 11c) and 15 h (Fig. 11d).

4. Conclusions and final remarks

Surface change of a cavitation erosion resistant steel (CA-6NM alloy) obtained by short time plasma nitriding (2 h) was investigated in the present work as a function of the high H_2 content in gas mixtures comprising 5–20% N_2 in volume, aiming to determine the effects on the morphology and constitution of the nitrided layer, and on the cavitation erosion behavior of the CA-6NM martensitic stainless steel treated surface. The main conclusions can be listed as follows:

- The N_2 content for high H_2 content gas mixtures (>80% H_2) strongly influences the phases' formation and its distribution on the nitrided layer for short nitriding time;
- The plasma nitrided layer obtained at 5% N_2 (+95% H_2) presents the finer and more homogeneous distribution of phases, comprising the nitrogen-containing tempered martensite and CrN, than the other studied conditions, leading to a better cavitation erosion resistance of the CA-6NM steel, at least to the conditions studied here;
- The worse cavitation erosion behavior verified for samples nitrided at 20% N_2 (+80% H_2) is supposed to be due to the formation of multiphase compound layer constituted by $Fe_4N + Fe_{2-3}N + CrN$, which can infer residual stress in treated surface.

Corrosion process study of the treated samples is to be done and it will be discussed in forthcoming publications. Finally, additional effort was also conducted aiming to determine the effects of the low temperature plasma nitriding on the surface characteristics and the cavitation erosion behavior of the CA-6NM steel samples, being that the results will be presented in future work.

Acknowledgments

The authors would like to acknowledge the Brazilian Agency CNPq for the financial support, the LORXI-UFPR for the XRD characterization, and LACTEC-UFPR for supplying the ASTM CA-6NM martensitic stainless steel.

References

[1] J.D. Crawford, CA6NM an update, in: Proceedings of the 29th Annual Steel Founder's Society of America Technical and Operating Conference, USA, 1974, pp. 1–13.
[2] T.G. Gooch, Heat treatment of welding 13%Cr–4%Ni martensitic stainless steel for sour service, Welding Research Supplement 74 (1995) 213–222.
[3] P.D. Bilmes, C.L. Llorente, I.J. Pérez, Toughness and microstructure of 13Cr4NiMo high strength steel welds, Journal of Materials Engineering and Performance 09 (2000) 609–615.
[4] Y.Y. Song, D.H. Ping, F.X. Yin, X.Y. Li, Y.Y. Li, Microstructural evolution and low temperature impact toughness of a Fe–13%Cr–4%Ni–Mo martensitic stainless steel, Materials Science and Engineering A 527 (2010) 614–618.
[5] L. Rayleigh, On the pressure developed in a liquid during the collapse of a spherical cavity, Philosophical Magazine 34 (1917) 94–98.
[6] M. Dular, B. Bachert, B. Stoffel, B. Sirok, Relationship between cavitation structures and cavitation damage, Wear 257 (2004) 1176–1184.
[7] C. Godoy, R.D. Mancosu, M.M. Lima, D. Brandão, J. Housden, J.C. Avelar-Batista, Influence of plasma nitriding and PAPVD $Cr_{1-x}N_x$ coating on the cavitation erosion resistance of an AISI 1045 steel, Surface and Coatings Technology 200 (2006) 5370–5378.
[8] C.E. Pinedo, W.A. Monteiro, On the kinetics of plasma nitriding a martensitic stainless steel type AISI 420, Surface and Coatings Technology 179 (2004) 119–123.
[9] P. Corengia, G. Ybarra, C. Moina, A. Cabo, E. Broitman, Microstructure and corrosion behaviour of DC-pulsed plasma nitrided AISI 410 martensitic stainless steel, Surface and Coatings Technology 187 (2004) 63–69.
[10] Y.-t. Xi, D.-x. Liu, D. Han, Improvement of corrosion and wear resistances of AISI 420 martensitic stainless steel using plasma nitriding at low temperature, Surface and Coatings Technology 202 (2008) 2577–2583.
[11] M.K. Sharma, B.K. Saikia, A. Phukan, B. Ganguli, Plasma nitriding of austenitic stainless steel in N_2 and N_2–H_2 dc pulsed discharge, Surface and Coatings Technology 201 (2006) 2407–2413.
[12] C.A. Figueroa, F. Alvarez, New pathways in plasma nitriding of metal alloys, Surface and Coatings Technology 200 (2005) 498–501.
[13] C.A. Figueroa, F. Alvarez, On the hydrogen etching mechanism in plasma nitriding of metals, Applied Surface Science 253 (2006) 1806–1809.
[14] S.F. Brunatto, J.L.R. Muzart, Influence of the gas mixture flow on the processing parameters of hollow cathode discharge iron sintering, Journal of Physics D: Applied Physics 40 (2007) 3937–3944.
[15] S.F. Brunatto, A.N. Allenstein, C.L.M. Allenstein, A.J.A. Buschinelli, Cavitation erosion behaviour of niobium, Wear 274–275 (2012) 220–228.
[16] M. Pohl, J. Stella, Quantitative CLSM roughness study on early cavitation-erosion damage, Wear 252 (2002) 501–511.
[17] K.Y. Chiu, F.T. Cheng, H.C. Man, Evolution of surface roughness of some metallic materials in cavitation erosion, Ultrasonics 43 (2005) 713–716.
[18] R.S. Mason, R.M. Allott, The theory of cathodic bombardment in a glow discharge by fast neutrals, Journal of Physics D: Applied Physics 27 (1994) 2372–2378.
[19] Y. Sun, T. Bell, A numerical model of plasma nitriding of low alloy steels, Materials Science and Engineering A 224 (1997) 33–47.
[20] F. Sanchette, E. Damond, M. Buvron, L. Henry, P. Jacquot, N. Randall, P. Alers, Single cycle plasma nitriding and hard coating deposition in a cathodic arc evaporation device, Surface and Coatings Technology 94–95 (1997) 261–267.
[21] F. Kieckow, C. Kwietniewski, E.K. Tentardini, A. Reguly, I.J.R. Baumvol, XPS and ion scattering studies on compound formation and interfacial mixing in TiN/Ti nanolayers on plasma nitrided tool steel, Surface and Coatings Technology 201 (2006) 3066–3073.
[22] A. Muñoz-Páez, J.I.F. Peruchena, J.P. Espinós, A. Justo, F. Castañeda, S. Díaz-Moreno, D.T. Bowron, Experimental evidences of new nitrogen-containing phases in nitrided steels, Chemistry of Materials 14 (2002) 3220–3222.
[23] W. Tuckart, E. Forlerer, L. Iurman, Delayed cracking in plasma nitriding of AISI 420 stainless steel, Surface and Coatings Technology 202 (2007) 199–202.